

Model Predictive Control Based Trajectory Optimization for Nap-of-the-Earth (NOE) Flight Including Obstacle Avoidance

Tiffany Lapp
Massachusetts Institute of Technology
tiff@mit.edu

Leena Singh, *Member, IEEE*
Draper Laboratory
lsingh@draper.com

Abstract – This paper presents a model predictive control based trajectory optimization method for Nap-of-the-Earth (NOE) flight including obstacle avoidance, emphasizing the mission objective of low altitude at high speed. A NOE trajectory reference is generated over a subspace of the terrain. It is then inserted into the cost function and the resulting trajectory tracking error term is weighted for more precise longitudinal tracking than lateral tracking through the introduction of the TF/TA ratio. Obstacle avoidance including preclusion of ground collision is accomplished through the establishment of hard state constraints. These state constraints create a ‘safe envelope’ within which the optimal trajectory can be found. Steps are taken to reduce complexity in the optimization problem including perturbational linearization in the prediction model generation and the use of control basis functions. Preliminary results over a variety of sample terrains are provided to show the mission objective of low altitude and high speed was met satisfactorily without terrain or obstacle collision, however, methods to preclude or deal with infeasibility must be investigated as speed is increased to and past 30 knots.

I. INTRODUCTION

SURVIVABILITY is a primary research objective for unmanned aerial vehicles. It is inherently obvious that as threat exposure increases, so does the probability of vehicle attrition. To effectively counter threat exposure, suitable guidance and control algorithms can take advantage of terrain masking through Nap-of-the-Earth (NOE) flight (less than 10m AGL) while simultaneously flying as fast as possible to enhance survivability if detected. This high speed requirement differentiates our research from traditional autonomous NOE flight which typically sacrifices velocity to attain fine altitude tracking. For such missions that involve cluttered, dangerous terrain, our high-speed, NOE flight objective translates to a highly constrained control problem. It is assumed that at low altitudes, the vehicle will be operating with an incomplete obstacle map which will be continuously updated with real-time sensor data. This motivates the need for an efficient algorithm for introducing new obstacle knowledge into the trajectory optimization to allow dynamic trajectory replanning.

To obtain the high accuracy tracking performance crucial to survival at the low altitudes defining NOE flight, optimal control is a prime candidate for trajectory

generation. However the high computational burden presented by optimal control is a known constraint on this control strategy. In attempt to reduce computational burden on the optimizer and take advantage of the “look ahead” that a human pilot is able to provide, predictive control was first proposed as a solution to the terrain following control problem in 1989 by [1]. Since then, there have been many applications of various forms of model predictive control (MPC) reaching beyond the terrain tracking problem to issues of trajectory optimization and obstacle avoidance, [2] – [4]. Specifically relating to this research effort, [3] applied non-linear model predictive control (NMPC) to combine the trajectory generation and tracking problems. They define a quadratic cost function with an output trajectory tracking error term, a control term and an additional term, introduced to bound the state variables that do not directly appear in the output. This cost is minimized subject to input constraints, guaranteeing physically realizable trajectories. In a 2-D urban terrain guidance and control problem, [4] utilized NMPC with hard constraints to accomplish obstacle avoidance. This research seeks to take advantage of the obstacle avoidance inherent with the application of hard state constraints and extend it to ground collision avoidance for NOE flight. It also seeks to combine the trajectory generation and tracking problems using MPC in a fashion that lends itself to real-time implementation and dynamic replanning based on sensor updates.

In the following research, a NOE trajectory reference is generated over a sample terrain at a nominal velocity. We define a cost function which introduces a Terrain Following / Terrain Avoidance (TF/TA) parameter similar to that of [5] allowing the user to adjust to what degree the reference trajectory is tracked longitudinally at the expense of the lateral tracking performance. This cost function is minimized by MPC subject to dynamic vehicle constraints, output constraints defined by a ‘safe’ envelope in the earth-frame and control input constraints. The resulting control sequence synthesizes a trajectory at 6 meters above the ground, which is guaranteed to preclude obstacle and terrain collisions, thus achieving our goal of high-speed, low altitude flight.

II. TRAJECTORY OPTIMIZATION USING MODEL PREDICTIVE CONTROL

Model predictive control (MPC) is a repeating, finite horizon optimal control scheme which uses an internal model of the plant dynamics (prediction model) to predict vehicle response and future states, thus minimizing the current error and optimizing the future trajectory within the prediction horizon [7, 8]. MPC produces a trajectory of control inputs to optimize the system states utilizing a quadratic form cost function similar to standard linear quadratic tracking. However, specific to finite horizon control, the cost is summed over the finite prediction horizon of time length $T_H = T_s * H$, rather than over an infinite time horizon. In this MPC formulation, the following cost is minimized to determine the optimal sequence of commands \mathbf{u}_k in the prediction horizon length H :

$$J_i = \sum_{k=i}^{i+H-1} (y_{k+1} - r_{k+1})^T Q_k (y_{k+1} - r_{k+1}) + u_k^T R_k u_k, \quad (1)$$

where \mathbf{y}_{k+1} is the output state at time t_{k+1} , \mathbf{r}_{k+1} is the state reference trajectory at time t_{k+1} , and Q_k and R_k are the tracking and control input weighting matrices in the horizon H . Once the control sequence has been determined, the first N (where N is a subinterval of H) inputs \mathbf{u}_i through \mathbf{u}_{i+N} are applied and the calculation is repeated. Thus, the selection of N determines the MPC rate. MPC literature has indicated that choosing an insufficient prediction horizon length T_H leads to instability [7, 9]; therefore a sufficiently long horizon (10 sec) was determined by tests and selected.

In this research, MPC plans trajectories for a 6-degree-of-freedom (6-DOF) helicopter between an initial and a final known set-point following the terrain and appropriately avoiding any obstacles encountered. To achieve this, some simplifications must be made as online optimization, even for a finite horizon, tends to be very computationally intensive [10]. To help reduce the problem size and alleviate the burden on the optimizer, two simplifications have been incorporated into the problem definition.

First, the prediction model is generated for MPC by perturbational linearization of the 6-DOF non-linear model about an updating nominal output and control trajectory. The nominal control (\mathbf{u}_0) is set as the trim controls for the initial iteration, and for every step thereafter it is updated as the output of the previous optimization cycle. The nominal output trajectory (\mathbf{y}_0) is calculated using the nonlinear input/output relationship defined in the helicopter model by integrating the helicopter equations of motion for each step in the horizon length, with initial conditions of the current position and the nominal control input.

With the nominal control and output trajectory established, perturbational analysis can be used to linearize the model around these trajectories. Perturbing the nonlinear model, $\dot{x} = F(x, u)$, the following is obtained:

$$\dot{x} = F_1(\dot{x}_0) + \delta\dot{x} = F_1(x_0, u_0) + \left. \frac{\partial F_1}{\partial x} \right|_{x_0, u_0} \delta x + \left. \frac{\partial F_1}{\partial u} \right|_{x_0, u_0} \delta u \quad (2)$$

$$y = F_2(x_0, u_0) + \delta y \quad (3)$$

$$\delta\dot{x} = A(x_0, u_0)\delta x + B(x_0, u_0)\delta u \quad (4)$$

$$\delta y = C(x_0, u_0)\delta x + D(x_0, u_0)\delta u \quad (5)$$

The optimizer is charged with finding the optimal linearized perturbational control, δu , from which $u = u_0 + \delta u$ can be found.

Second, to further decrease complexity, rather than explicitly calculating $A(x_0, u_0)$, $B(x_0, u_0)$, $C(x_0, u_0)$ and $D(x_0, u_0)$ for each step along the horizon, an input-output mapping is constructed using a set of *control basis functions*, similar to those described in [4]. Control basis functions are predefined sequences of controls prescribed for the length of the predictive horizon.

Given these predefined sequences, the complexity of the optimization problem can be greatly reduced with comparable performance by charging the optimizer to find scale factors (α) for the basis functions as opposed to finding a separate control for each step along the horizon. For this work, we have selected tent functions consisting of a positive slope ramp up to a peak followed by a negative slope ramp back down to zero, as plotted in Fig. 1. Two second pulse widths were determined by simulation to adequately reduce complexity while maintaining performance standards.

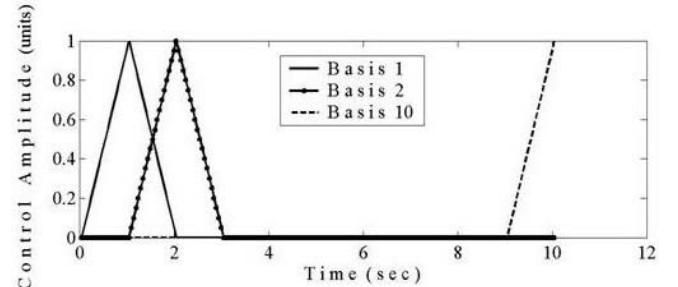


Fig. 1. Sample basis function control sequences for a 10 second prediction horizon.

The input-output mapping is created by using the linearity between input and output. The vector δu is simply a linear combination of the basis functions:

$$\begin{bmatrix} \delta u_k \\ \vdots \\ \delta u_{k+H-1} \end{bmatrix} = \begin{bmatrix} du & 0 & 0 & 0 & 0 \\ 2du & \ddots & \vdots & \vdots & \vdots \\ \vdots & \ddots & du & 0 & \vdots \\ 2du & \ddots & 2du & \ddots & 0 \\ du & \ddots & \vdots & \ddots & du \\ 0 & \ddots & 2du & \ddots & 2du \\ 0 & 0 & du & \ddots & \vdots \\ \vdots & \vdots & \vdots & \ddots & 2du \\ 0 & 0 & 0 & 0 & du \end{bmatrix} \begin{bmatrix} \alpha_1 \\ \alpha_2 \\ \alpha_3 \\ \alpha_4 \\ \alpha_5 \end{bmatrix} \quad (6)$$

$$\delta u = B \alpha \quad (6A)$$

$$= [\mathbf{b}_1, \mathbf{b}_2 \dots \mathbf{b}_5] \alpha \quad (6B)$$

Based on our linear model, the output $\delta\mathbf{y}$ would be the same linear combination of each basis function output, \mathbf{s}_n , which is simply the vector output of each basis function after it has been input to our nonlinear system model. Thus as $\delta\mathbf{u} = \mathbf{B}\boldsymbol{\alpha}$, $\delta\mathbf{y} = \mathbf{S}\boldsymbol{\alpha}$ where $\mathbf{S} = [\mathbf{s}_1, \mathbf{s}_2 \dots \mathbf{s}_5]$.

The cost function can then be described in terms of the nominal and perturbed states: $\mathbf{y} = \mathbf{S}\boldsymbol{\alpha} + \mathbf{y}_0$ and $\mathbf{u} = \mathbf{B}\boldsymbol{\alpha} + \mathbf{u}_0$ yielding:

$$J_i = \sum_{k=i}^{i+H-1} \left[\begin{array}{l} (\mathbf{S}\boldsymbol{\alpha} + \mathbf{y}_0 - \mathbf{r}_{k+1})^T \mathbf{Q}_k (\mathbf{S}\boldsymbol{\alpha} + \mathbf{y}_0 - \mathbf{r}_{k+1}) \\ + (\mathbf{B}\boldsymbol{\alpha} + \mathbf{u}_0)^T \mathbf{R} (\mathbf{B}\boldsymbol{\alpha} + \mathbf{u}_0) \end{array} \right] \quad (7)$$

This will be revisited in section V which discusses the implementation of the reference trajectory and performance objectives within the cost.

III. TERRAIN FOLLOWING REFERENCE TRAJECTORY GENERATION

To establish the reference trajectory from which the actual trajectory will be subtracted in the cost function, we follow what is typical to most terrain following systems and start with an initial waypoint and a final waypoint, using a straight line path between the two as our first guess at a nominal 2D trajectory. The z-dimension is inserted from elevation data corresponding to each (x,y) reference coordinate. The terrain following reference path is set at the desired distance, 6 meters for this case, above the ground level along our 2D trajectory. Finally, the complete reference trajectory is synthesized by sampling our 3D reference trajectory at the simulation rate assuming the nominal velocity selected for the simulation. In addition to the earth frame reference trajectory including x, y and z, a Ψ reference was added to assert vehicle attitude.

IV. CONSTRAINT BASED OBSTACLE AVOIDANCE

Recent obstacle avoidance strategies make use of two main ideas: reference trajectory modification to produce or enhance obstacle avoidance response [4,11] and/or definition of ‘safe envelope’ (either by hard or soft constraints) within which the new trajectory is to be planned, [4,5,6]. Our method uses the ‘safe envelope’ idea. To handle obstacles, we define a constraint free, convex feasible space that excludes the obstacle and terrain spaces and constrain the optimizer to produce the sequence of controls (H-interval long) that produce spatial trajectories within this feasible solution space. This assures obstacle and terrain collision avoidance. In addition to the terrain itself, this research deals with two types of obstacles: trees which require the helicopter to fly around them, and utility wires which require overflight. (For this study, flight under wires is not considered a feasible solution.) Laterally, the convex feasible set is defined to constrain the optimizer to search for a path in an obstacle free subspace by setting an upper and/or lower bound determined from the location of the closest obstacles in range, (Fig. 2, $t = t3$). If multiple obstacles are detected within this radius for a given point,

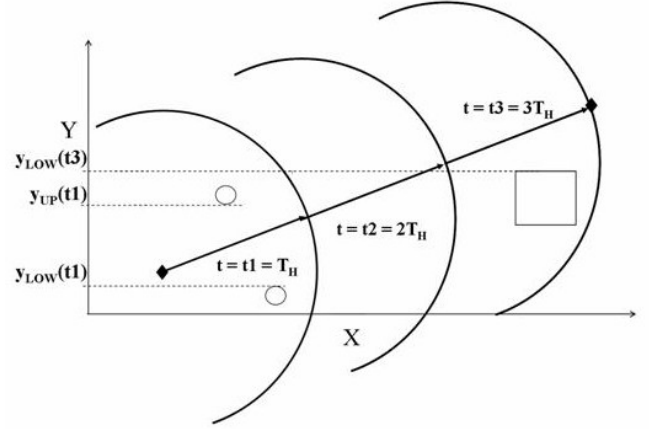


Fig.2. Constraint application method for obstacle avoidance where $y_{LOW}(t)$ and $y_{UP}(t)$ are the lower and upper bounds set on y in the MPC loop at time t.

the closest upper obstacle is set as the upper limit for that particular point and the closest lower obstacle is set as the lower limit, (Fig. 2, $t = t1$). When obstacles requiring a longitudinal response are detected within the prediction horizon radius ($T_H * V_{NOM}$ meters), the obstacle height plus safety margin is set as a lower bound for that point, no lateral constraints are imposed. If no longitudinal-response obstacles are detected, the minimum allowable altitude above ground is set to preclude ground collision. For the purposes of this application, a hard upper limit for altitude is never set although a threat defined maximum altitude limit similar to the lateral map limits could easily be imposed. Soft constraints in the cost function stipulate that the optimizer maintain reference altitude which can be weighted for more precise longitudinal tracking than lateral tracking through the TF/TA ratio, discussed in detail in section V.

We convert the output spatial constraints into constraints on the control scale factors, $\boldsymbol{\alpha}$. Since the optimizer is being charged to find scale factors for each control basis function, the relationships derived in section 3; $\mathbf{u} = \mathbf{B}\boldsymbol{\alpha} + \mathbf{u}_0$ and $\mathbf{y} = \mathbf{S}\boldsymbol{\alpha} + \mathbf{y}_0$, are inserted to express all output, state and control input constraints in terms of $\boldsymbol{\alpha}$. This yields the traditional form:

$$\begin{bmatrix} \mathbf{S} \\ \mathbf{B} \end{bmatrix} \boldsymbol{\alpha} \leq \begin{bmatrix} \mathbf{y}_{lim} - \mathbf{y}_0 \\ \mathbf{u}_{lim} - \mathbf{u}_0 \end{bmatrix} \quad (8)$$

V. MISSION OBJECTIVE INCLUSION INTO THE COST FUNCTION MINIMIZATION

The performance objectives of low altitude and high speed are folded into the optimization problem through the desired reference trajectory (\mathbf{r}), however, note this is also enforced through the selection of TF/TA ratio, ω , within the state weighting term, Q. Within \mathbf{Q}_k , set for each time-step k along the prediction horizon, the x, y and Ψ weights are set to 1 and the z weight is set to ω : $\mathbf{Q}_k = [1, 1, \omega, 1]$. A high value for ω here will allow little deviation from the set altitude about ground while allowing the xy-track to

meander. A smaller value will emphasize lateral tracking while not attending as highly to maintaining the precise distance above ground, (a safety margin will be enforced by constraints in either case). It is worth noting additionally that any performance objectives could be folded in here, making MPC online optimization a very versatile and effective way to deal with real-time reconfiguration and control needs. When the cost function described in (7) is minimized subject to the constraints defined in the previous section, the resulting scaled controls synthesize a trajectory with minimal deviation from the reference trajectory while avoiding encountered obstacles and terrain features.

VI. SIMULATION

A. Vehicle Model

The vehicle selected for this research is the Yamaha R-50 helicopter. Standard helicopter non-linear equations of motion were obtained and R-50 mass properties were inserted. These equations were linearized for use within MPC as the prediction model described in section II. In simulation, the resulting MPC trajectory/constraint generator and controller were applied to the non-linear dynamics; however, no outside disturbances (wind, weather, failures) have been simulated so far. Thus for the results presented, the only difference between the internal model and the actual plant are the errors in perturbational linearization. Future work will include application of these algorithms to a high fidelity helicopter model. For this simulation, the MPC loop was run at 2 Hz to compute the 20 Hz controls. We assume full state feedback, eliminating the need for an estimator. In future work, disturbance rejection and the effects of state estimation will be investigated as well as the possible addition of an inner loop stability augmentation system.

The control constraints that were placed on the vehicle (and converted to constraints on the scaling factors, α) are the following:

$$\begin{array}{llll} 0G & \leq & \text{Main Rotor Thrust} & \leq 3\frac{1}{2}G \\ -20^\circ & \leq & \text{Pitch Cyclic} & \leq 20^\circ \\ -20^\circ & \leq & \text{Roll Cyclic} & \leq 20^\circ \\ -\frac{1}{2}G & \leq & \text{Tail Rotor Thrust} & \leq \frac{1}{2}G \end{array}$$

B. Specific Problem Definition

In this simulation, our optimizer choice, SQOPT (software available at <http://www.sbsi-sol-optimize.com/>), was charged with finding the optimal control trajectory (using control basis function scale factors) to fly the helicopter down two different terrain cross sections taken from the area around Mt. Adams in Washington State, appropriately avoiding any obstacles detected along the way. From the input latitudinal and longitudinal coordinates, the appropriate portion of the online Digital Terrain Elevation Data (DTED) Level 0 map was extracted and interpolated to 12.5 meter resolution. Ultimately it is expected that this information will be augmented with real-time terrain sensor feedback data which will replace our

interpolation. The interpolated data is then converted to Cartesian coordinates with the origin set at the initial waypoint, and (x,y,z) corresponding to (latitude, longitude, altitude). Then at each timestep, through the Euler angles, the body velocities are rotated to the earth-frame allowing the reference of 6 meters above terrain to be specified and tracked in the earth-frame. We set the TF/TA ratio $\omega = 10$ to enforce the desired altitude reference.

C. Obstacles

The interpolated terrain was populated randomly with the two different types of obstacles; lateral obstacles (trees, poles, etc.), modelled as cylinders which require ‘go-around’ obstacle avoidance response, and longitudinal obstacles (utility wires, etc.), modelled as walls which require ‘go-over’ obstacle avoidance response. For this study, it is assumed that sensor information is preprocessed to provide MPC with obstacle location and size information (including the discernment between lateral or longitudinal required obstacle responses) within a 150 meter radius of our vehicle.

VII. RESULTS

A. Tracking

As mentioned in the problem definition, tracking performance was evaluated in this research over a range of terrain sections. These sections were selected measuring their relative difficulties by the change in required flight path angles commanded over the prediction horizon. The first piece of terrain selected for investigation is marked by relatively low maximum flight path angle magnitudes (maximum of 40°) and little overall deviation in the terrain slope. Fig. 3 shows the simulation data plotted against the actual terrain at 10 and 20 knot nominal velocities and Fig. 4 exhibits the respective tracking errors, defined to be the difference between the achieved position and the reference position. Predictably, given their linear references, the lateral tracking shows average tracking errors in X and Y of approximately 1 meter with maximum errors of 3 meters. Doubling the nominal velocity from 10 to 20 knots does not significantly attenuate the tracking performance, however, when the terrain severity increases with the second terrain section, we expect to see a degradation of performance with increase in nominal velocity. Though it is not immediately clear in the 3D plot of the trajectory, the error plot shows clearly that longitudinal (Z) reference tracking is very accurate even at nominal velocities of 20 knots, with an average tracking error of approximately 1 meter with a maximum error of less than 3 meters. These higher altitude tracking errors entered in the steepest climb and descent phases of the terrain traversing the slopes near the end of the reference path. As for the higher nominal velocities of 25 and 30 knots, the optimization became infeasible when the helicopter encountered required flight path angles greater than $\sim 30^\circ$ in the reference terrain. This

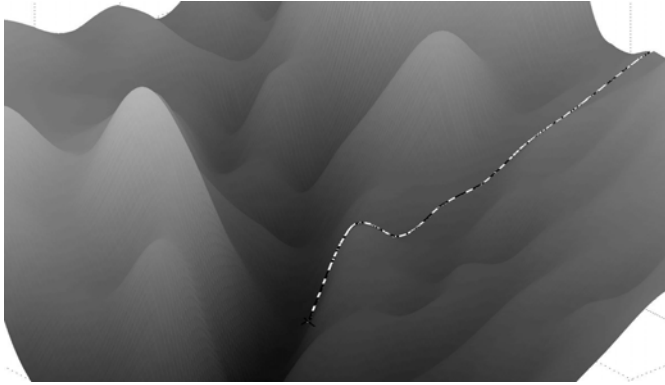


Fig. 3. Terrain Section 1 plotted with simulation data at 10 and 20 knot nominal velocities. White line = 10 knots, Black dashed line = 20 knots.

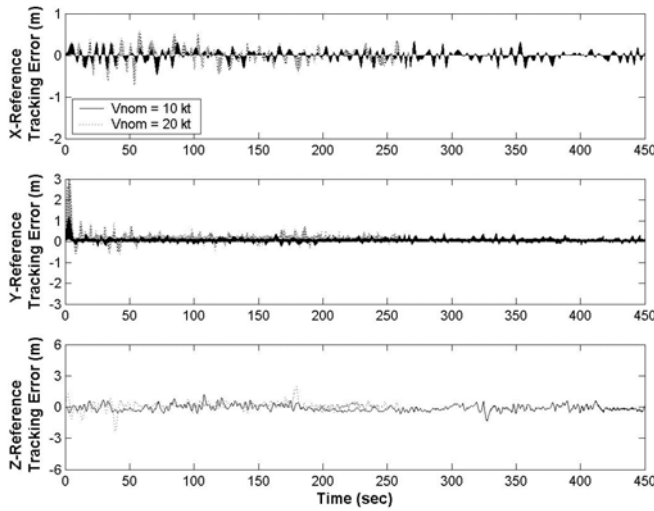


Fig. 4. Terrain Section 1 reference tracking errors in X, Y and Z for 10 and 20 knot nominal velocities.

is not entirely unexpected as we observe an increase in tracking error as the nominal velocity increased. This becomes more pronounced as the more severe cross section is traversed. We hypothesize that at the higher flight path angles, we approach the limits of the helicopter maneuverability at high speeds. The published helicopter limits show that helicopter maneuverability crests at a certain operational speed then rapidly decays due to quicker vehicle control saturation associated with increase in speed. We believe that increasing the prediction horizon via an increased sensor range at these higher velocities would aid in preventing this infeasibility.

The second terrain section was selected due to its extreme (increasing steadily in magnitude to $\sim 60^\circ$) flight path angle requirements. Fig. 5 shows simulation data plotted against the actual terrain at 10 and 20 knot nominal velocities and Fig. 6 shows a plot of the tracking error for each axis, X, Y, and Z, as previously defined. As expected, this terrain resulted in degraded tracking performance in all three axes compared to the first terrain section. Lateral tracking exhibited higher errors overall, specifically in the sections when altitudes approached the hard constraints.

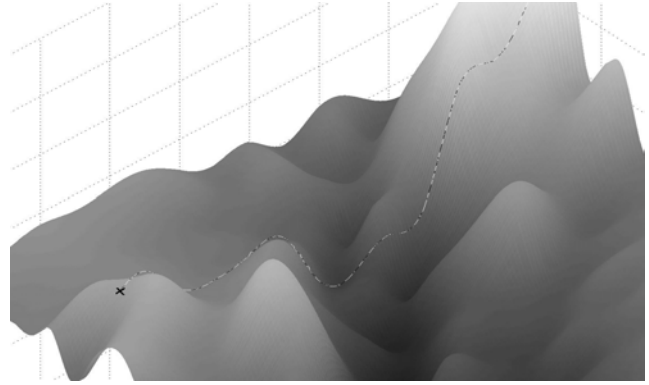


Fig. 5. Terrain Section 2 plotted with simulation data at 10 and 20 knot nominal velocities. White line = 10 knots, Black dashed line = 20 knots.

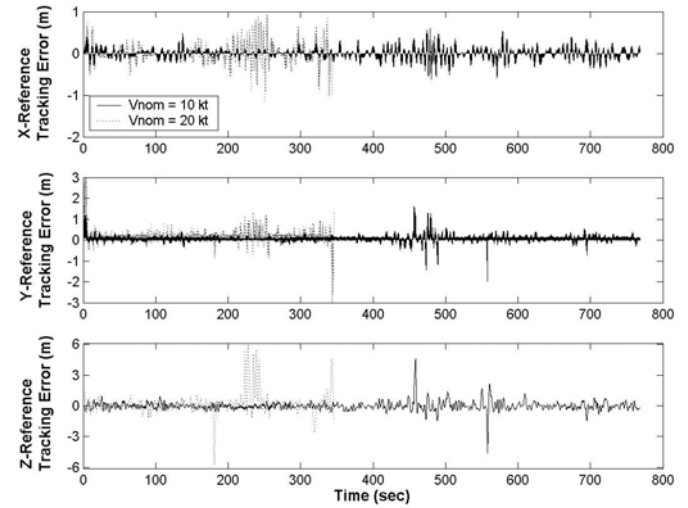


Fig. 6. Terrain Section 2 reference tracking errors in X, Y and Z for 10 and 20 knot nominal velocities.

This shows that the choice of TF/TA ratio was effective as when longitudinal tracking approached the constraints, lateral tracking which remained relatively unconstrained, was sacrificed to maintain feasibility. The altitude tracking errors approach but never exceed the hard ground constraint, therefore the application of hard minimum altitude constraints has proven to be effective to prevent ground collision. In actual application of this constraint, a safety margin allowing for the size of the vehicle should be added to the actual terrain height.

As with terrain section 1, nominal velocities of 25 and 30 knots aborted their optimizations due to infeasibility as they met the more severe flight path angle requirements. As an extension of this paper, the next area of our research will involve infeasibility investigation and formulation of formal tuning suggestions for MPC parameters (horizon lengths and cost weightings) in order to achieve desired performance over extreme changes in required flight path angle.

B. Obstacle Avoidance

The helicopter successfully avoided all obstacles without violation of the set safety margins at the nominal velocities

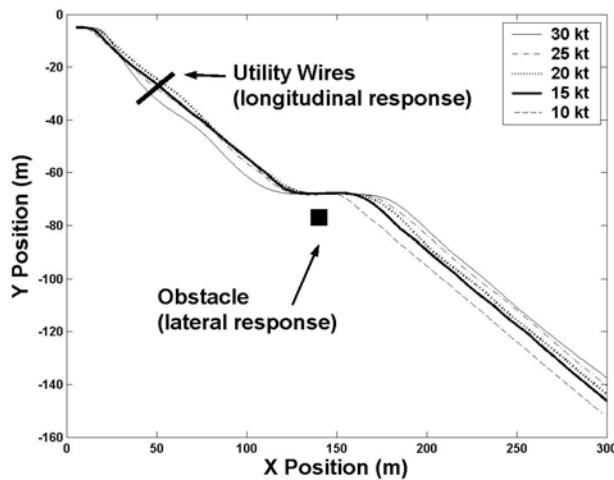


Fig. 7: Y Position vs. X Position Close-up of Lateral Obstacle Avoidance and Reference Regeneration with varying speeds

tested. The reference trajectory was redrawn successfully in the lateral obstacle case so that the new shortest distance between the endpoint and the current position became the updated reference track. Fig. 7 shows a bird's eye view of the lateral obstacle avoidance and reference regeneration.

Longitudinal obstacle avoidance was not quite as straightforward as lateral obstacle avoidance in implementation. The discontinuous jump of the constraint from 6 meters above terrain to the obstacle height upon encountering a longitudinal obstacle initially caused infeasibility. Even though the actual trajectory would begin to anticipate the change in constraints, the anticipation was not fast enough get the helicopter altitude above the lower limit altitude constraint by the time the constraint was enforced. To remedy this, the reference trajectory was updated upon obstacle detection to reflect the presence of the obstacle and smooth the discontinuity in altitude. This proved to be an effective method of longitudinal obstacle avoidance at all tested speeds as safety margins were maintained above and around the obstacle and the reference height above ground was recaptured once the longitudinal obstacle was passed. Fig. 8 shows a close-up of longitudinal obstacle avoidance at varying nominal velocities.

VIII. CONCLUSIONS

This paper presented a model predictive control based trajectory optimization method for Nap-of-the-Earth flight at 6m above ground level which precludes collision with the ground, terrain features and obstacles. The mission objectives of low altitude and high speed were met with success; however, our nominal velocity variation testing revealed performance degradation as speed is increased to and past 25 knots. For speeds of 25 knots and greater, it may be advisable to adjust the cost function weights, use a longer prediction horizon, increase the control update rate or increase the desired altitude above ground so that larger tracking errors can be tolerated. Future research is planned

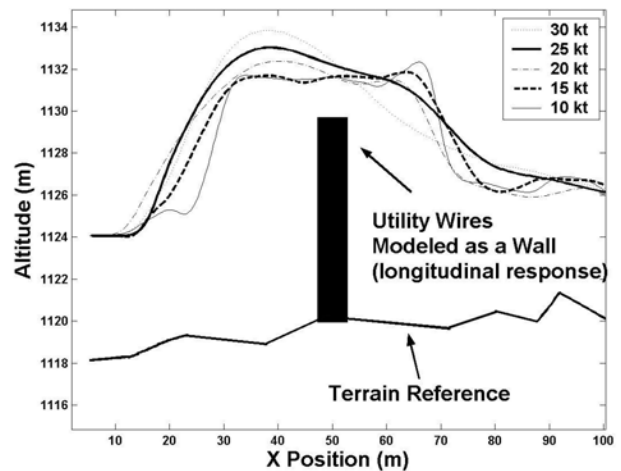


Fig. 8: Altitude vs. X Position Close-up of Longitudinal Obstacle Avoidance with Varying speeds

to investigate the sensitivities of performance in the 25 knot to 60 knot range to these four parameters.

IX. REFERENCES

- [1] R. Hess, Y. Jung, "An Application of Generalized Predictive Control to Rotorcraft Terrain-Following Flight," *IEEE Trans. Systems, Man and Cybernetics*, vol. 19, no. 5, Sept.-Oct 1989, pp 955-962.
- [2] A. Bogdanov, E. Wan, M. Carlsson, Y. Zhang, R. Kiebertz, A. Baptista, "Model Predictive Neural Control of a High Fidelity Helicopter Model," AIAA Guidance, Navigation, and Control Conference and Exhibit, Montreal, Canada, Aug. 6-9, 2001, AIAA Paper AIAA-2001-4164.
- [3] H. Kim, D. Shim, S. Sastry, "Nonlinear Model Predictive Tracking Control for Rotorcraft-based Unmanned Aerial Vehicles," *Proceedings of the 2002 American Control Conference*, vol. 5, 8-10 May 2002, pp 3576 - 3581.
- [4] L. Singh, J. Fuller, "Trajectory Generation for a UAV in Urban Terrain, using Nonlinear MPC," *Proceedings of the 2001 American Control Conference*, vol. 3, 25-27 June 2001, pp 2301 - 2308.
- [5] R. Denton, J. Jones, P. Froberg, "Demonstration of an Innovative Technique for Terrain Follow/Terrain Avoidance - The Dynapath Algorithm," *Proceedings of the IEEE 1985 National Aerospace and Electronics Conference*, 20-24 May, 1985, pp 522-529.
- [6] R. Coppenbarger, "Sensor-Based Automated Obstacle-Avoidance System for NOE Rotorcraft Missions," *Proceedings of SPIE Head-Mounted Displays*, vol. 2735, June 1996, pp 221 - 232.
- [7] J. Maciejowski, *Predictive Control with Constraints*, Prentice Hall, NY; 2002
- [8] C. Garcia, D. Prett, M. Morari, "Model Predictive Control: Theory and practice - a survey," *Automatica*, vol. 25, 1989.
- [9] D. Mayne, J. Rawlings, C. Rao, and P. Scokaert, "Constrained model predictive control: Stability and optimality," *Automatica*, vol. 36, 2000, pp. 789 - 814.
- [10] A. Bemporad, F. Borrelli, M. Morari, "The Explicit Solution of Constrained LP-Based Receding Horizon Control," *Proceedings of the 39th IEEE Conference on Decision and Control*, vol. 1, 12-15 Dec 2000, pp 632 - 637.
- [11] V. Cheng, T. Lam, "Automatic Guidance and Control Laws for Helicopter Obstacle Avoidance," *Proceedings of the 1992 International Conference on IEEE Robotics and Automation*, vol. 1, 12-14 May 1992, pp 252 - 260.